Enhancing the Scattering Induced by Gold Periodic Arrays Over Optical Waveguides Through Indium Tin Oxide Buffer Layers

Rita Asquini, *Member, IEEE*, Alessio Buzzin, Nicolas Hanine, Alessia Mannetta, Badrul Alam, and Vincenzo Ferrara

***Abstract*—This article presents the optical analysis on how the light coupling performance between optical channel waveguides and gold periodic nanoarrays in the visible spectrum can be improved using an indium tin oxide (ITO) thin film as buffer layer. Coupling efficiency, out-of-plane scattering and far-field projected beam focus and diffraction angle are evaluated using Finite-Difference Time-Domain (FDTD) method and scattering theory for different nanogratings and nanocylinders array patterns. The implementation of ITO enables up to a 12 fold increase in coupling efficiency, a 6.4 fold enhancement of light scattered out of the array plane and consequent improvements in the diffracted beam radiation intensity peaks, without compromising the beam's focus or altering its deflection angle. This configuration provides a cheap and simple solution to increase the device performance without changing the array features, for integrated biosensing and scattering-related applications.**

***Index Terms*—Arrays, FDTD, gold, gratings, indium tin oxide, optical coupling, optical waveguides, periodic structures, scattering.**

I. Introduction

PERIODIC nanostructures have been widely researched in the field of optics as promoters of phenomena such as light scattering and diffraction [1], [2], [3]. In integrated photonics, planar nanogratings coupled with optical waveguides exploit the diffraction phenomenon for routing portions of the guided light in and out of the optical chip [4], [5], [6], [7]. In plasmonics, light interaction with 2D metal periodic nanoarrays is used for surface plasmon resonance (SPR) and induces phenomena such as fluorescence, dichroism, and Raman scattering [8], [9], [10]. Such structures are implemented for applications spanning from signal treatment and routing, to biomolecular sensing, at times aided by chemical functionalization [11], [12], [13], [14].

Manuscript received 30 November 2023; revised 15 February 2024; accepted 23 February 2024. Date of publication 4 March 2024; date of current version 4 April 2024. This work was supported by the European Union under the Italian National Recovery and Resilience Plan (NRRP) of Next Generation EU, PNRR MUR project PE00000023-NQSTI (the National Quantum Science and Technology Institute), by the Sapienza Research Project RP1221816BF94E0A "Liqui-LOC" and by the European Union under the Italian National Recovery and Resilience Plan (NRRP) of Next Generation EU, partnership on "Telecommunications of the Future" (PE00000001—Program "RESTART"). *(Corresponding author: Rita Asquini.)*.

The authors are with the Department of Information Engineering, Electronics and Telecommunications, "Sapienza" University of Rome, 00184 Rome, Italy (e-mail: rita.asquini@uniroma1.it; alessio.buzzin@uniroma1.it; nicolas.hanine@uniroma1.it; alessia.mannetta@uniroma1.it; badrul.alam@uniroma1.it; vincenzo.ferrara@uniroma1.it).

Digital Object Identifier 10.1109/JPHOT.2024.3371289

Low loss optical channel waveguides can be obtained with different fabrication procedures and different materials, such as SU-8 polymer [15], diffused ion-exchanged on glass and other composite materials [16], [17], [18]. Such waveguiding structures can be efficiently used to fabricate simple and cost effective integrated optical devices working in a wide frequency spectrum for optical communication and sensing systems [19], [20], [21].

Coupling efficiency, scattering losses, diffraction angle, projected beam intensity and focus are considered as key features in controlled scattering and diffraction, and they can be finely tuned by adjusting shape, period, pitch and thickness of the selected structures [22], [23]. Some applications may require an ex-post enhancement and/or tuning of the projected light beam radiation intensity, or an improvement of the waveguide-array coupling: this can be achieved through accurate adjustments in the design and fabrication phases [24], such as refining details in the array pattern, changing the thickness of the material, or modulating the etch-depth [25], [26], [27]. These could represent critical challenges: considering the subwavelength scale of such structures, any mistakes in improving one feature could compromise the others.

This paper studies the performances of a thin film of indium tin oxide (ITO) as optical buffer layer between channel waveguides and periodic nanostructures; the arrangement provides a low cost and simple solution to enhance optical coupling, scattering losses and far-field radiation intensity of the diffracted beam. A numerical assessment is presented, involving gold (Au) periodic subwavelength nanoarray patterns on a SU-8 waveguide in the visible spectrum. Results are presented for 4 different array configurations placed either upon the ITO buffer film or directly on the underlying low-index waveguide. The changes caused by ITO in the waveguide-array interaction are analyzed in terms of optical coupling. The study is completed evaluating also the change in the amount of guided light scattered out of the array plane and its far-field projected beam focus, radiation intensity peaks and angle in the selected cases. This work aims at providing solutions for applications where an enhancing, or a fine-tuning, of the optical coupling between integrated optical channels and overlying metal nanostructures is required. As an example, in optical biosensing fields, the nature and amount of interaction with the analyte sample could be monitored by finely controlling the amount of light hitting the nanostructures [28],

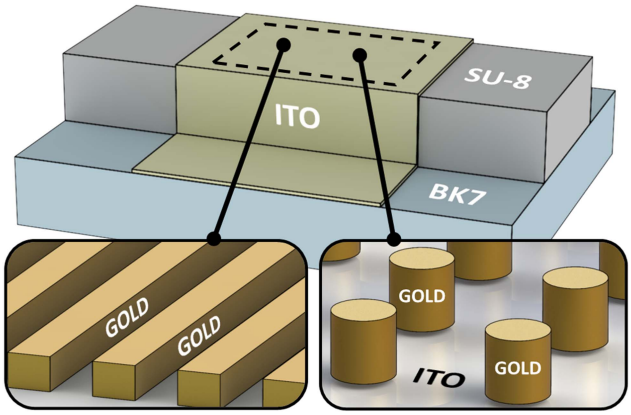

Fig. 1. Schematic view of the structure under analysis. The two insets show the details of the two configurations of gold periodic array: nanograting (left inset) and nanocylinders (right inset).

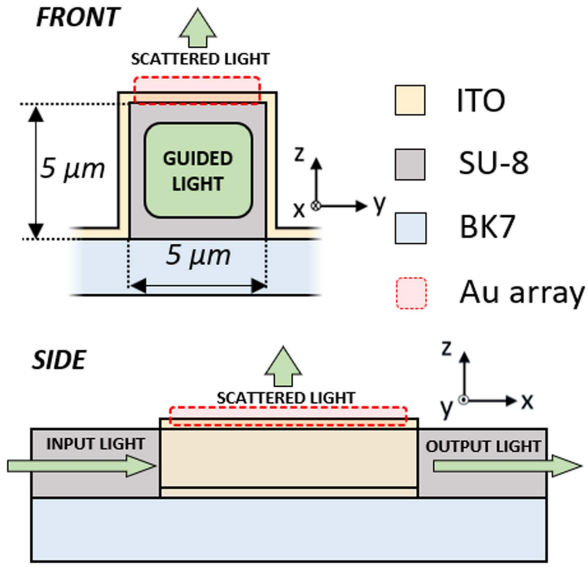

Fig. 2. Front view (top left) and side view (bottom) of the system modeled for the numerical analyses.

[29]. Furthermore, other applications include redirecting light out of the plane for optical communications purposes, where specific amounts of the guided light may be extracted and routed to secondary paths [30].

II. Investigated Structures

A SU-8 polymer structure (5 μm-thick and 5 μm-wide) acts as optical waveguide in the visible spectrum [31] (refractive index equal to 1.59 at 540 nm wavelength, from Microchem SU-8 3000 datasheets). The waveguide is placed onto a BK7 glass substrate (n=1.52 at $\lambda = 540$ nm, from Schott glass datasheets), and the whole device is immersed in water (n = 1.33 at $\lambda = 540$ nm [32]). Two different configurations of Au periodic nanostructures are alternatively placed on top of such waveguide, both covering a 100 μm-long path for a total coating footprint of (5·100) μm^2, in four different configurations: the first two consist of 1D-periodic nanogratings (100 nm thickness) with a period equal to 240 nm and 360 nm respectively, and a one-to-one ratio between empty and full states (i.e. 50% duty cycle); the third and the fourth configurations are 2D-periodic patterns of nanocylinders (100 nm thick with 50 nm radius), disposed with an array pitch of 250 nm and 350 nm respectively. Each configuration is investigated with and without an ITO thin film (n = 1.87 at $\lambda = 540$ nm [33]), acting as buffer layer between the SU-8 waveguide and the nanostructures. A qualitative sketch of the structure is depicted in Fig. 1. As this work aims at providing solutions for a wide range of applications, the system structure has been kept basic and simple, and multiple nanostructures arrangements have been investigated. As nanostructures' material, Au was chosen as it allows an easy chemical functionalization with a wide variety of species, making such configuration suitable for diverse optical biosensing systems [34], [35]. 1D periodic diffraction gratings were chosen as, both in optical communications and optical sensing, they represent the simplest and most common tool for redirecting light out of the optical waveguide to secondary paths [2]. 2D periodic nanocylinders arrays were chosen as they have been already studied for light scattering and diffraction, and as tools for biosensing applications [9], [36]. Taking into consideration all the parameters of the system, such as working wavelength, refractive index and shape of the materials, Au structures having periods around 350 nm and 250 nm are capable of redirecting light at about 90° angle with respect to the guided light flow direction, and at about 120° angle with respect to the guided light flow direction, respectively [2], [37]. Moreover, Au nanocylinders with a pitch of 250 nm and a diameter of 100 nm have been proven to optimize focus, collimation and directionality of the diffracted beams in integrated optics, enhancement of fluorescence in biosensing applications with similar configurations [9], [38].

III. Simulation Model

Starting from the front view and the side view sketched at the top and bottom of Fig. 2, three-dimensional models were patterned, considering a 5 μm-thick and 5 μm-wide waveguide cross-section. The side view's left boundary of the SU-8 domain was considered as the waveguide input. The selected wavelength range of the light excitation spans from 490 nm to 590 nm, with 2 nm steps (50 steps). The input light mode is TM fundamental, as it has been proved to better interact with periodic arrays of gold nanostructures in this specific configuration [9]. Maxwell's equations for the electromagnetic field were implemented in a Finite-Difference Time-Domain (FDTD) model, using Ansys Lumerical as simulation software. The 3D model was meshed down to (10·10·5) nm^3 sub-domains in the ITO and nanostructures regions. The boundary conditions of the model were set as PML (Perfectly Matched Layers).

The presented study deals with observing changes in the amount of light exiting the system through the integrated waveguide and/or redirected out of the chip's plane when optical buffer films are interposed between the waveguide and overlying nanostructures: for this purpose, here we focused on analyzing the optical power fluxes through the waveguide input, the

waveguide output and the upper boundary of the modeled system, without focusing on modal analyses and input/output modal changes. We analyzed the coupling efficiency between SU-8 and nanoarrays: the difference among the input guided power P_{in} and the output guided power P_{out} can be considered as the power absorbed by the system, and it can be determined as follows:

$$P_{in} - P_{out} = P_{guide} + P_{ITO} + P_{array} + P_{scat} \quad (1)$$

P_{in} is partially absorbed into the waveguide (P_{guide}) and into the ITO layer (P_{ITO}), a part is lost due to scattering from the surface of the waveguide (P_{scat}), and a portion is absorbed/scattered by the Au array (P_{array}). Since the analysis is carried out in the visible spectrum, P_{guide} and P_{ITO} have been neglected, due to the optical transparency of both ITO and SU-8 [39], [40]. Moreover, P_{scat} corresponds to propagation losses of about 10^{-4} dB/cm and is small enough to be ignored as well. With these concepts taken into consideration, and since this study focuses on the waveguide/array interaction, the input-output power decrease can be mainly attributed to the amount of optical power coupled from the SU-8 waveguide to the Au array. The coupling efficiency can be then obtained from the normalized difference between the guided optical power, considered as the surface integral of the Poynting vector through the surface of the waveguide cross-section, calculated at the input interface (side-view's left boundary of the SU-8 domain) and at the output interface (side view's right boundary of the SU-8 domain):

$$\text{Coupling Efficiency}\,[\%] = \frac{P_{in} - P_{out}}{P_{in}} \cdot 100 \quad (2)$$

In addition to this, to evaluate the portion of guided light scattered out of the array's plane, the evolution of the optical power along the side view of the simulated models is compared. With the same logic of (2), but considering P_{up} as the light transmitted through a XY plane 5 μm over the arrays, the scattered light can be evaluated as follows:

$$\text{Scattered light}\,[\%] = \frac{P_{up}}{P_{in}} \cdot 100 \quad (3)$$

Finally, the far-field analysis is used to study the deflection angle, focus and radiation intensity of the light scattered from the arrays.

IV. Results

A. Coupling Efficiency Analysis

Firstly, the SU-8/ITO optical coupling was analyzed at 540 nm wavelength excitation (i.e. green light). Fig. 3(a) plots the coupling efficiency between the SU-8 waveguide and the ITO films with thicknesses ranging from 0 to 525 nm. Peaks and valleys of coupling efficiency occur with about 250 nm periodicity [21], [41]: peaks can be observed when ITO thickness is equal to 125 nm (3.5%) and 375 nm (4.75%); valleys can be observed at approximately 250 nm and 475 nm. Increasing the ITO thickness means to increase the optical power absorbed in the ITO film (P_{ITO}). Therefore, 125 nm is chosen as optimal thickness for an ITO buffer layer for an enhanced optical coupling, minimizing at the same time the losses due to ITO absorption.

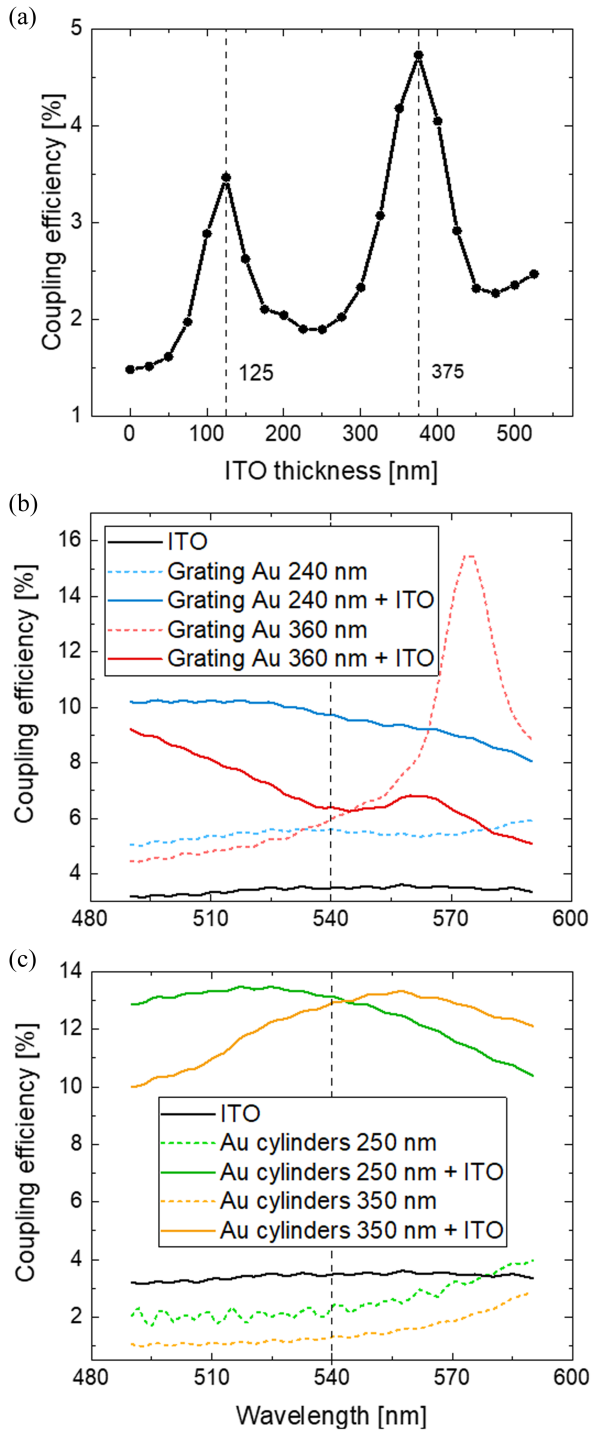

Fig. 3. Coupling efficiency between SU-8 waveguide and ITO thin-films, with ITO thickness spanning from 0 to 525 nm (a). Coupling efficiency between SU-8 waveguide and nanogratings (b) or nanocylinders arrays (c) with and without 125 nm-thick ITO buffer layer.

Subsequently, the coupling efficiency analysis is conducted considering the two configurations of Au grating and two configurations of Au nanocylinders array, with and without the 125 nm-thick ITO buffer layer. The study is carried out with an excitation wavelength range between 490 nm and 590 nm (i.e. with 540 nm as central point and a 100 nm span). As Fig. 3(b) shows, the

125 nm-thick ITO buffer layer enhances the optical coupling between the waveguide and the 240 nm Au grating by 1.7 times (i.e. from 5.6% to 9.7%) at 540 nm. At the same wavelength, the coupling with the 360 nm grating increases by a factor 1.1 (from 6% to 6.4%). The plot in Fig. 3(b) clearly shows that, in the case of the 240 nm period, the enhancement decreases as the wavelength increases. On the other hand, the 360 nm Au grating with ITO experiences an enhancement in optical coupling only from 490 nm to 550 nm of working wavelength; for longer wavelengths the effect is reversed, with ITO damaging the optical coupling: at 580 nm the coupling efficiency is about 5.5% with ITO and reaches up to 12.4% without ITO. Fig. 3(c) plots the coupling efficiency in the nanocylinder arrays configuration. It is clearly visible that the sole array has less capability of coupling light than the sole ITO layer in the whole considered wavelength spectrum for both array pitches. When the ITO buffer layer is implemented under the 250 nm-pitched nanocylinders array, the enhancement reaches a factor 6.75 (from 2% to 13.5%) at wavelengths shorter than 540 nm, a factor 5 (from 2.5% to 13%) at 540 nm and decreases for longer wavelengths, but never being less than 2.7 times (from 3.9% to 10.4%) at 590 nm wavelength. The 350 nm-pitched array also benefits from the ITO buffer layer, with a 10 to 12 fold increase for wavelengths shorter than 540 nm, a 12 fold increase (from 1% to 12%) at 540 nm and a 6 fold increase (from 2% to 12%) at 590 nm wavelength.

B. *Scattered Light Analysis*

Fig. 4 shows the comparison of the evolution of the guided optical power through the waveguide in the considered configurations. Fig. 4(a)–(d) all share the same optical power scale. The longitudinal section (i.e. the side view, see the bottom part of Fig. 2) of each model has been inspected, and the chromatic scale has been set in logarithmic mode to highlight the scattered light contributions, which in the studied cases are significantly smaller with respect to the main light contribution, flowing through the SU-8 domain from left to right. The Au structures cause the scattering of a portion of the guided light out of the array plane. The 240 nm grating and the 360 nm grating do not benefit from the underlying ITO thin film as visible from Fig. 4(a) and (b). Instead, both the 250 nm-pitched (Fig. 4(c)) and the 350 nm-pitched (Fig. 4(d)) Au nanocylinders arrays show an improvement with the ITO layer.

Using (3) the enhancement of the scattered losses is evaluated numerically. Both Au gratings display no significant change of scattered losses when implementing the ITO buffer film (less than 10% decrease in the case of 360 nm and less than 10% increase in the case of 240 nm). The results show a 6.4 fold enhancement in the case of 350 nm-pitched nanocylinders array and a 2.7 fold increase of scattered light in the case of 250 nm-pitched nanocylinders array due to the presence of the ITO thin film. Not all of the coupled light is scattered along the preferred direction, some is reflected back to the substrate and a small portion is diffracted in different directions. Structures that feature the thin film ITO exhibit an additional peak due to the interface between the ITO layer and the water.

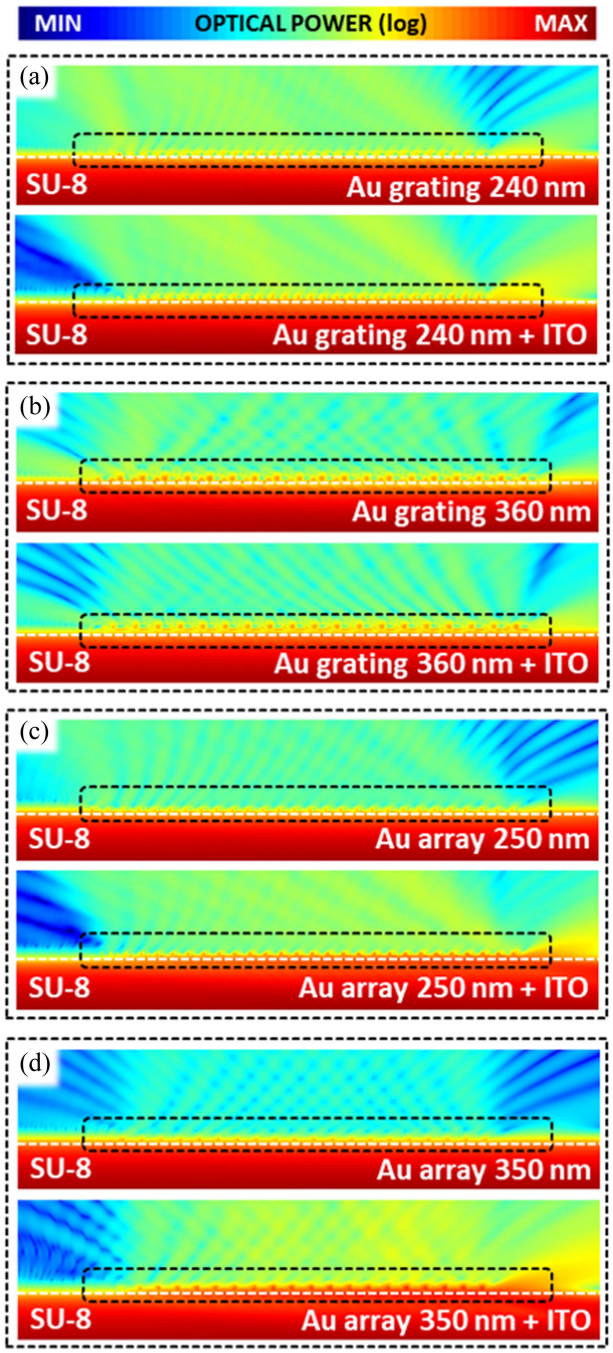

Fig. 4. Evolution of the optical power inside the four configurations of the studied device, comparison of the side view between the standard versions and the ITO-buffered versions: Au 240 nm grating (a), Au 360 nm grating (b), Au 250 nm-pitched nanocylinders array (c), and Au 350 nm-pitched nanocylinders array (d). The scale has been set to logarithmic to emphasize the out-of-plane scattered light contributions.

C. *Far-Field Analysis*

Fig. 5 plots the scattered light's intensity and deflection angle projected over the array plane (XY plane), considering the z>0 hemisphere, where $\theta = 0$ corresponds to the z-axis, perpendicular to the array plane. Each comparison (Fig. 5(a)–(d)) is plotted with its own dimensional scale to better highlight the differences.

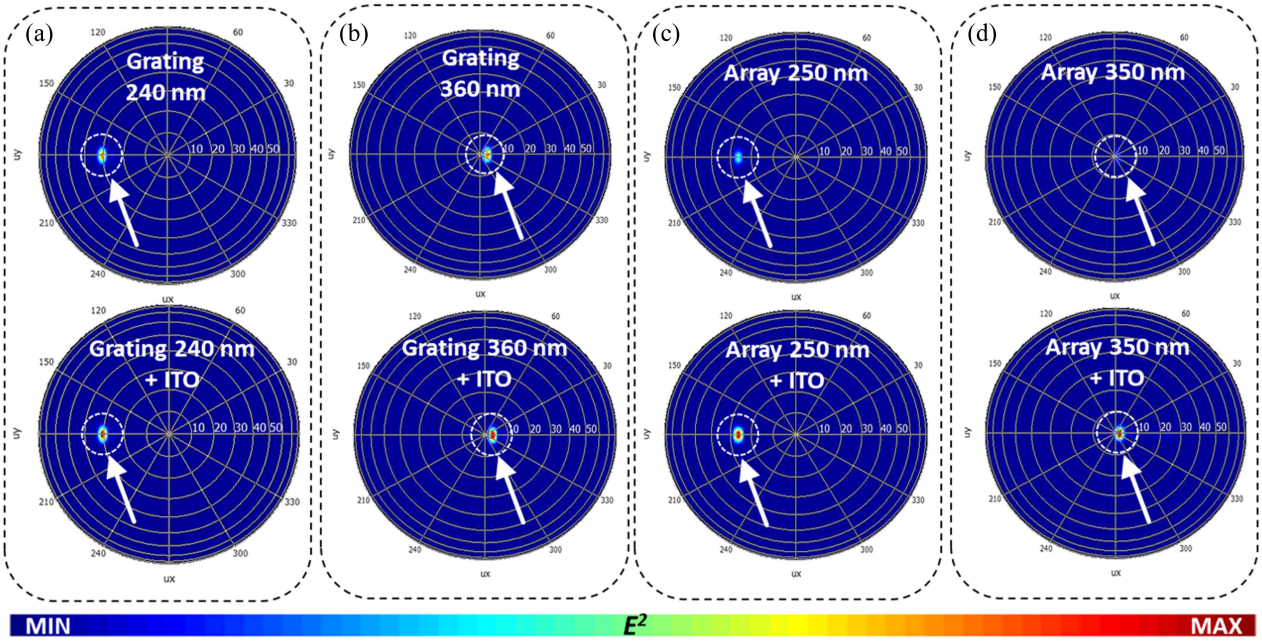

Fig. 5. Far-field projection of the scattered light beam focus, intensity and angle in the four studied configurations: comparison between the ITO and non-ITO results: Au 240 nm grating (a), Au 360 nm grating (b), Au 250 nm-pitched nanocylinders (c), and Au 350 nm-pitched nanocylinders array (d). The far-field is monitored in the XY plane projected over the arrays. The graphs are in spherical coordinates and refer to the upper hemisphere ($z > 0$) of the model.

All the periodic structures show a highly collimated and directional beam (unlike the sole ITO uniform thin film, which does not exhibit diffraction characteristics). Structures with similar pitches show similar diffraction angles. In particular, the 240 nm grating and the 250 nm-pitched array exhibit a beam deflection with a peak around 30° with respect to the z-axis, while the 360 nm grating and the 350 nm-pitched array grating cause a nearly vertical deflection (peak at less than 5° with respect to the z-axis). The results highlight that the presence of the ITO thin film does not induce a significant variation in beam collimation and directionality. Moreover, the presence of ITO increases the intensity of the luminous beam only in the nanocylinders arrays case, and it does not promote any significant changes in the gratings, confirming the scattered light analysis results (Section IV-B).

V. Conclusion

In this work, ITO thin films are studied as optical buffer layers to be implemented in waveguiding devices where a simple and low-cost tool for enhancing optical coupling and optical scattering is desired. For this purpose, devices made by a SU-8 polymer waveguide coated with Au periodic arrays are modelled, with different shapes and configurations. Simulations are carried out by means of FDTD in the visible spectrum to evaluate the difference in behavior with and without the ITO buffer layer, in terms of waveguide-array optical coupling, amount of out-of-plane scattered optical power and far-field diffracted beam radiation intensity peak, focus and angle. The reported results show how the ITO can promote significantly more optical coupling between the underlying waveguide and the overlying structures. The amount of light scattered out of the arrays' plane increases from the presence of ITO: the 240 nm grating reaches enhancement peaks of about 2 times, but the enhancement is relatively low for the 360 nm-pitched grating at 540 nm wavelength. Over 5 fold coupling enhancement in the case of the 250 nm-pitched nanocylinders array and a 12 fold coupling increase in the case of the 350 nm-pitched nanocylinders array are calculated at 540 nm wavelength with respect to standard waveguide-array configurations. The far-field analysis shows how neither the diffracted beam's focus nor its diffraction angle are affected from the ITO buffer layer in any of the studied configurations, but the radiation intensity peaks greatly improve when ITO is implemented. As the outcomes show, Au periodic structures can benefit from ITO buffer layers by experiencing an increase in coupled optical power from the underlying waveguide without compromising the diffracted beam's focus nor its diffraction angle. However, attention must be paid on the array's period and on the working wavelength, as in some cases ITO may be detrimental and harm the coupling efficiency. In case of sensing applications where the Au array is required to act as substrate for chemical functionalization, such as in the field of integrated scattering-induced fluorescence [9], ITO buffer layers may represent a double sensitivity enhancer: the demonstrated increase in optical coupling pairs with the increase in overall surface for chemical functionalization, being ITO easy to functionalize (besides gold) with a broad spectrum of chemical species [42], [43], [44]. Furthermore, a thin-film ITO coating through physical vapor deposition can represent a low-cost, simple and fast enhancement/fine-tuning tool in the case of off-chip optical routing, as optimizing the amount of deflected optical power may represent a time-costly re-design of the patterns, or a technological challenge if critical features need to be re-adjusted in the fabrication phase.

REFERENCES

[1] M. G. Moharam and T. K. Gaylord, "Rigorous coupled-wave analysis of planar-grating diffraction," *J. Opt. Soc. Amer.*, vol. 71, no. 7, pp. 811–818, 1981.

[2] T. Gaylord and M. Moharam, "Analysis and applications of optical diffraction by gratings," *Proc. IEEE*, vol. 73, no. 5, pp. 894–937, May 1985.

[3] K. Busch, G. Von Freymann, S. Linden, S. F. Mingaleev, L. Tkeshelashvili, and M. Wegener, "Periodic nanostructures for photonics," *Phys. Rep.*, vol. 444, no. 3, pp. 101–202, 2007.

[4] J. E. Harvey and R. N. Pfisterer, "Understanding diffraction grating behavior: Including conical diffraction and Rayleigh anomalies from transmission gratings," *Opt. Eng.*, vol. 58, no. 8, 2019, Art. no. 087105.

[5] Q. K. Xia and D. N. Wang, "Optical fiber diffraction gratings," *IEEE Photon. Technol. Lett.*, vol. 34, no. 3, pp. 177–180, 2022.

[6] R. K. Sinha, M. Mojahedi, and C. Ozcan, "Highly-efficient apodized grating coupler in visible spectrum for backward coupling," in *Proc. IEEE Photon. Conf.*, 2022, pp. 1–2.

[7] M. Guizzardi, S. Bonfadini, L. Moscardi, I. Kriegel, F. Scotognella, and L. Criante, "Large scale indium tin oxide (ITO) one dimensional gratings for ultrafast signal modulation in the visible spectral region," *Phys. Chem. Chem. Phys.*, vol. 22, no. 13, pp. 6881–6887, 2020.

[8] S. Kasani, K. Curtin, and N. Wu, "A review of 2D and 3D plasmonic nanostructure array patterns: Fabrication, light management and sensing applications," *Nanophotonics*, vol. 8, no. 12, pp. 2065–2089, 2019.

[9] B. Alam, A. Ferraro, R. Caputo, and R. Asquini, "Optical properties and far field radiation of periodic nanostructures fed by an optical waveguide for applications in fluorescence and raman scattering," *Opt. Quantum Electron.*, vol. 54, no. 5, 2022, Art. no. 307.

[10] A. Veroli et al., "High circular dichroism and robust performance in planar plasmonic metamaterial made of nano-comma-shaped resonators," *J. Opt. Soc. Amer. B*, vol. 36, no. 11, pp. 3079–3084, 2019.

[11] C. Valsecchi and A. G. Brolo, "Periodic metallic nanostructures as plasmonic chemical sensors," *Langmuir*, vol. 29, no. 19, pp. 5638–5649, 2013.

[12] M. C. Estevez, M. Alvarez, and L. M. Lechuga, "Integrated optical devices for lab-on-a-chip biosensing applications," *Laser Photon. Rev.*, vol. 6, no. 4, pp. 463–487, 2012.

[13] M. A. Badshah, N. Y. Koh, A. W. Zia, N. Abbas, Z. Zahra, and M. W. Saleem, "Recent developments in plasmonic nanostructures for metal enhanced fluorescence-based biosensing," *Nanomaterials*, vol. 10, no. 9, 2020, Art. no. 1749.

[14] F. Chiavaioli, F. Baldini, S. Tombelli, C. Trono, and A. Giannetti, "Biosensing with optical fiber gratings," *Nanophotonics*, vol. 6, no. 4, pp. 663–679, 2017.

[15] A. Buzzin, R. Asquini, D. Caputo, and G. De Cesare, "Sensitive and compact evanescent-waveguide optical detector for sugar sensing in commercial beverages," *Sensors*, vol. 23, no. 19, 2023, Art. no. 8184.

[16] A. D'Alessandro, R. Asquini, R. P. Bellini, D. Donisi, and R. Beccherelli, "Integrated optic devices using liquid crystals: Design and fabrication issues," *Proc. SPIE*, vol. 5518, pp. 123–135, 2004.

[17] A. D'Alessandro, B. Bellini, D. Donisi, R. Beccherelli, and R. Asquini, "Nematic liquid crystal optical channel waveguides on silicon," *IEEE J. Quantum Electron.*, vol. 42, no. 10, pp. 1084–1090, 2006.

[18] S. Ertman et al., "Periodic liquid crystalline waveguiding microstructures," *Sci. Rep.*, vol. 13, no. 1, 2023, Art. no. 13896.

[19] A. Piccardi et al., "Trends and trade-offs in nematicon propagation," *Appl. Phys. B*, vol. 104, no. 4, pp. 805–811, 2011.

[20] R. Asquini, C. Chiccoli, P. Pasini, L. Civita, and A. D'Alessandro, "Low power photonic devices based on electrically controlled nematic liquid crystals embedded in poly(dimethylsiloxane)," *Liquid Crystals*, vol. 45, no. 13/15, pp. 2174–2183, 2018.

[21] R. Asquini, A. Buzzin, D. Caputo, and G. De Cesare, "Integrated evanescent waveguide detector for optical sensing," *IEEE Trans. Compon. Packag. Manuf. Technol.*, vol. 8, no. 7, pp. 1180–1186, 2018.

[22] D. Taillaert et al., "Grating couplers for coupling between optical fibers and nanophotonic waveguides," *Japanese J. Appl. Phys., Part 1: Regular Papers Short Notes Rev. Papers*, vol. 45, no. 8, pp. 6071–6077, 2006.

[23] Z. Zhang et al., "Efficiency enhanced grating coupler for perfectly vertical fiber-to-chip coupling," *Materials*, vol. 13, no. 12, 2020, Art. no. 2681.

[24] A. D. Simard and S. LaRochelle, "A dynamic model of silicon Bragg grating modulators," *IEEE J. Sel. Topics Quantum Electron.*, vol. 22, no. 6, 2016, Art. no. 3400109.

[25] Y. Wang, X. Fu, Y. Chen, L. Qin, Y. Ning, and L. Wang, "The development progress of surface structure diffraction gratings: From manufacturing technology to spectroscopic applications," *Appl. Sci.*, vol. 12, no. 13, 2022, Art. no. 6503.

[26] N. V. Sapra et al., "Inverse design and demonstration of broadband grating couplers," *IEEE J. Sel. Topics Quantum Electron.*, vol. 25, no. 3, May/Jun. 2019, Art no. 6100207.

[27] Y. Zou, S. Chakravarty, W.-C. Lai, C.-Y. Lin, and R. T. Chen, "Methods to array photonic crystal microcavities for high throughput high sensitivity biosensing on a silicon-chip based platform," *Lab Chip*, vol. 12, no. 13, pp. 2309–2312, 2012.

[28] C. Chen and J. Wang, "Optical biosensors: An exhaustive and comprehensive review," *Analyst*, vol. 145, no. 5, pp. 1605–1628, 2020.

[29] M. Elsherif et al., "Optical fiber sensors: Working principle, applications, and limitations," *Adv. Photon. Res.*, vol. 3, no. 11, 2022, Art. no. 2100371.

[30] L. Cheng, S. Mao, Z. Li, Y. Han, and H. Fu, "Grating couplers on silicon photonics: Design principles, emerging trends and practical issues," *Micromachines*, vol. 11, no. 7, 2020, Art. no. 666.

[31] A. Buzzin, R. Asquini, D. Caputo, and G. De Cesare, "Evanescent waveguide lab-on-chip for optical biosensing in food quality control," *Photon. Res.*, vol. 10, no. 6, pp. 1453–1461, 2022.

[32] G. M. Hale and M. R. Querry, "Optical constants of water in the 200-nm to 200-μm wavelength region," *Appl. Opt.*, vol. 12, no. 3, pp. 555–563, 1973.

[33] T. A. F. König et al., "Electrically tunable plasmonic behavior of nanocube–polymer nanomaterials induced by a redox-active electrochromic polymer," *ACS Nano*, vol. 8, no. 6, pp. 6182–6192, 2014.

[34] P. M. Tiwari, K. Vig, V. A. Dennis, and S. R. Singh, "Functionalized gold nanoparticles and their biomedical applications," *Nanomaterials*, vol. 1, no. 1, pp. 31–63, 2011.

[35] F. Petronella et al., "Label-free and reusable antibody-functionalized gold nanorod arrays for the rapid detection of Escherichia coli cells in a water dispersion," *Environ. Sci.: Nano*, vol. 9, no. 9, pp. 3343–3360, 2022.

[36] S. Klinghammer et al., "Plasmonic biosensor based on vertical arrays of gold nanoantennas," *ACS Sensors*, vol. 3, no. 7, pp. 1392–1400, 2018.

[37] S. A. Maier et al. *Plasmonics: Fundamentals and Applications*, vol. 1. New York, NY, USA: Springer, 2007.

[38] N. Mahi et al., "In depth investigation of lattice plasmon modes in substrate-supported gratings of metal monomers and dimers," *J. Phys. Chem. C*, vol. 121, no. 4, pp. 2388–2401, 2017.

[39] D. Caputo et al., "Chromatography system based on amorphous silicon sensor," *J. Non-Crystalline Solids*, vol. 354, no. 19, pp. 2615–2618, 2008.

[40] A. Buzzin, R. Asquini, D. Caputo, and G. De Cesare, "On-glass integrated SU-8 waveguide and amorphous silicon photosensor for on-chip detection of biomolecules: Feasibility study on hemoglobin sensing," *Sensors*, vol. 21, no. 2, 2021, Art. no. 415.

[41] A. Mannetta, A. Buzzin, N. Hanine, B. Alam, V. Ferrara, and R. Asquini, "Coupling efficiency enhancement between SU-8 waveguides and plasmonic nanostructures through indium tin oxide thin films," *2023 International Conference on Numerical Simulation of Optoelectronic Devices (NUSOD)*, Turin, Italy, 2023, pp. 5–6.

[42] I. I. Suni, "Substrate materials for biomolecular immobilization within electrochemical biosensors," *Biosensors*, vol. 11, no. 7, 2021, Art. no. 239.

[43] E. B. Aydın and M. K. Sezgintürk, "Indium tin oxide (ITO): A promising material in biosensing technology," *TrAC Trends Anal. Chem.*, vol. 97, pp. 309–315, 2017.

[44] E. Zor, I. Hatay Patir, H. Bingol, and M. Ersoz, "An electrochemical biosensor based on human serum albumin/graphene oxide/3-aminopropyltriethoxysilane modified ITO electrode for the enantioselective discrimination of D- and l-tryptophan," *Biosensors Bioelectron.*, vol. 42, pp. 321–325, 2013.

Open Access funding provided by 'Università degli Studi di Roma "La Sapienza" 2' within the CRUI CARE Agreement